

# A brief introduction to cosmic topology

M.J. Rebouças

*Centro Brasileiro de Pesquisas Físicas  
Rua Dr. Xavier Sigaud 150  
22290-180 Rio de Janeiro - RJ, Brazil*

**Abstract.** Whether we live in a spatially finite universe, and what its shape and size may be, are among the fundamental long-standing questions in cosmology. These questions of topological nature have become particularly topical, given the wealth of increasingly accurate astro-cosmological observations, especially the recent observations of the cosmic microwave background radiation. An overview of the basic context of cosmic topology, the detectability constraints from recent observations, as well as the main methods for its detection and some recent results are presented.

## 1. INTRODUCTION

Whether the universe is spatially finite and what is its shape and size are among the fundamental open problems that the modern cosmology seeks to resolve. These questions of topological nature have become particularly topical, given the wealth of increasingly accurate astro-cosmological observations, especially the recent observations of the cosmic microwave background radiation (CMBR) [1]. An important point in these topological questions is that as a (local) metrical theory general relativity leaves the (global) topology of the universe undetermined. Despite this inability to predict the topology of the universe at a classical level, we should be able to devise strategies and methods to detect it by using data from current or future cosmological observations.

The aim of these lecture notes is to give a brief review of the main topics on cosmic topology addressed in four lectures in the XI<sup>th</sup> Brazilian School of Cosmology and Gravitation, held in Mangaratiba, Rio de Janeiro from July 26 to August 4, 2004. Although the topics had been addressed with some details in the lectures, here we only intend to present a brief overview of the lectures. For more details we refer the readers to the long list of references at the end of this article.

The outline of this article is as follows. In section 2 we discuss how cosmic topology arises in the context of the standard Friedmann–Lemaître–Robertson–Walker (FLRW) cosmology, and what is the main observational physical effect used in the search for a nontrivial topology of the spatial section of the universe. We also recall in this section some relevant results about spherical and hyperbolic 3-manifolds, which will be useful in the following sections. In section 3 we discuss the detectability of cosmic topology, present examples on how one can decide whether a given topology is detectable or not according to recent observations, and review some important results on this topic. In section 4 we review the two main statistical methods to detect cosmic topology from the distribution of discrete cosmic sources. In section 5 we describe two methods devised for the search of signs of a non-trivial topology in the CMBR maps.

## 2. BASIC CONTEXT

General relativity (GR) relates the matter content of the universe to its geometry, and reciprocally the geometry constrains the dynamics of the matter content. As GR is a purely metrical (local) theory it does not fix the (global) topology of spacetime. To illustrate this point in a very simple way, imagine a two-dimensional (2–D) world and its beings. Suppose further these 2–D creatures have a geometrical theory of gravitation [an (1 + 2) spacetime theory], and modelling their universe in the framework of this theory they found that the 2–D geometry of the regular space is Euclidean — they live in a spatially flat universe. This knowledge, however, does not give them enough information

to determine the space topology of their world. Indeed, besides the simply-connected Euclidean plane  $\mathbb{R}^2$ , the space section of their universe can take either of the following multiply-connected space forms: the cylinder  $\mathbb{C}^2 = \mathbb{R} \times \mathbb{S}^1$ , the torus  $\mathbb{T}^2 = \mathbb{S}^1 \times \mathbb{S}^1$ , the Klein bottle  $\mathbb{K}^2 = \mathbb{S}^1 \times \mathbb{S}^1_\pi$  and the Möbius band  $\mathbb{M}^2 = \mathbb{R} \times \mathbb{S}^1_\pi$ . In brief, the local geometry constrains, but does not dictate the topology of the space. This is the very first origin of cosmic topology in the context of GR, as we shall discuss in what follows.

Within the framework of the standard FLRW cosmology in the context of GR, the universe is modelled by a 4 – manifold  $\mathcal{M}$  which is decomposed into  $\mathcal{M} = R \times M$ , and is endowed with a locally isotropic and homogeneous Robertson–Walker (RW) metric

$$ds^2 = -dt^2 + a^2(t) [d\chi^2 + f^2(\chi)(d\theta^2 + \sin^2 \theta d\phi^2)] , \quad (1)$$

where  $f(\chi) = (\chi, \sin \chi, \text{or } \sinh \chi)$  depending on the sign of the constant spatial curvature ( $k = 0, 1, -1$ ), and  $a(t)$  is the scale factor.

The spatial section  $M$  is usually taken to be one of the following simply-connected spaces: Euclidean  $\mathbb{E}^3$  ( $k = 0$ ), spherical  $\mathbb{S}^3$  ( $k = 1$ ), or hyperbolic  $\mathbb{H}^3$  ( $k = -1$ ) spaces. However, since geometry does not dictate topology, the 3-space  $M$  may equally well be any one of the possible quotient manifolds  $M = \tilde{M}/\Gamma$ , where  $\Gamma$  is a discrete and fixed point-free group of isometries of the covering space  $\tilde{M} = (\mathbb{E}^3, \mathbb{S}^3, \mathbb{H}^3)$ . In forming the quotient manifolds  $M$  the essential point is that they are obtained from  $\tilde{M}$  by identifying points which are equivalent under the action of the discrete group  $\Gamma$ . Hence, each point on the quotient manifold  $M$  represents all the equivalent points on the covering manifold  $\tilde{M}$ . The action of  $\Gamma$  tessellates (tiles)  $\tilde{M}$  into identical cells or domains which are copies of what is known as fundamental polyhedron (FP). An example of quotient manifold in three dimensions is the 3–torus  $T^3 = \mathbb{S}^1 \times \mathbb{S}^1 \times \mathbb{S}^1 = \mathbb{E}^3/\Gamma$ . The covering space clearly is  $\mathbb{E}^3$ , and a FP is a cube with opposite faces identified as indicated, in figure 1, by the equal opposite letters. This FP tiles the covering space  $\mathbb{E}^3$ . The group  $\Gamma = \mathbb{Z} \times \mathbb{Z} \times \mathbb{Z}$  consists of discrete translations associated with the face identifications.

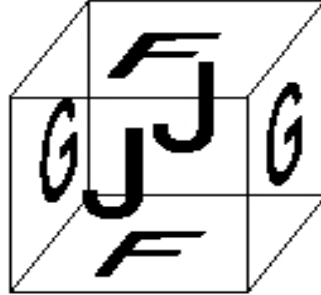


**FIGURE 1.** A fundamental polyhedron of the Euclidean 3–torus. The opposite faces are identified by the matching through translations of the pairs of equal opposite letters.

In a multiply connected manifold, any two given points may be joined by more than one geodesic. Since the radiation emitted by cosmic sources follows (space-time) geodesics, the immediate observational consequence of a non-trivial spatial topology of  $M$  is that the sky may (potentially) show multiple images of radiating sources: cosmic objects or specific correlated spots of the CMBR. At large cosmological scales, the existence of these multiple images (or pattern repetitions) is a physical effect often used in the search for a nontrivial 3-space topology.<sup>1</sup> In this article, in line with the usage in the literature, by cosmic topology we mean the topology of the space section  $M$  of the space-time manifold  $\mathcal{M}$ .

A question that arises at this point is whether one can use the topological multiple images of the same celestial objects such as cluster of galaxies, for example, to determine a nontrivial cosmic topology (see, e.g., refs [2] – [8]) In practice, however, the identification of multiple images is a formidable observational task to carry out because it

---

<sup>1</sup> Clearly we are assuming here that the radiation (light) must have sufficient time to reach the observer from multiple directions, or put in another way, that the universe is sufficiently ‘small’ so that this repetitions can be observed. In this case the observable horizon  $\chi_{hor}$  exceeds at least the smallest characteristic size of  $M$ . A more detailed discussion on this point will be given in section 3.

involves a number of problems, some of which are:

- Two images of a given cosmic object at different distances correspond to different periods of its life, and so they are in different stages of their evolutions, rendering problematic their identification as multiple images.
- Images are seen from different angles (directions), which makes it very hard to recognize them as identical due to morphological effects;
- High obscuration regions or some other object can mask or even hide the images;

These difficulties make clear that a direct search for multiples images is not very promising, at least with available present-day technology. On the other hand, they motivate new search strategies and methods to determine (or just detect) the cosmic topology from observations. Before discussing in section 4 the statistical methods, which have been devised to search for a possible nontrivial topology from the distribution of discrete cosmic sources, we shall discuss in the next section the condition for detectability of cosmic topology.

### 3. DETECTABILITY OF COSMIC TOPOLOGY

In this section we shall examine the detectability of cosmic topology problem for the nearly flat ( $\Omega_0 \sim 1$ ) universes favored by current observation [9], and show that a number of important results may be derived from the very fact that the cosmic topology is detectable. Thus, the results present in this section are rather general and hold regardless of the cosmic topology detection method one uses, as long as it relies on images or pattern repetitions.

The extent to which a nontrivial topology of may or may not be detected for the current bounds on the cosmological density parameters has been examined in a few articles [10] – [20]. The discussion below is based upon our contribution to this issue [10] – [13].

In order to state the conditions for the detectability of cosmic topology in the context of standard cosmology, we note that for non-flat metrics of the form (1), the scale factor  $a(t)$  can be identified with the curvature radius of the spatial section of the universe at time  $t$ . Therefore  $\chi$  is the distance of a point  $p = (\chi, \theta, \phi)$  to the coordinate origin  $O$  (in the covering space) in units of the curvature radius, which is a natural unit of length that shall be used throughout this paper.

The study of the detectability of a possible non-trivial topology of the spatial section  $M$  requires a topological typical length which can be put into correspondence with observation survey depths  $\chi_{obs}$  up to a redshift  $z = z_{obs}$ . A suitable characteristic size of  $M$ , which we shall use in this paper, is the so-called injectivity radius  $r_{inj}$ , which is nothing but the radius of the smallest sphere ‘inscribable’ in  $M$ , and is defined in terms of the length of the smallest closed geodesics  $\ell_M$  by  $r_{inj} = \ell_M/2$  (see fig. 2).

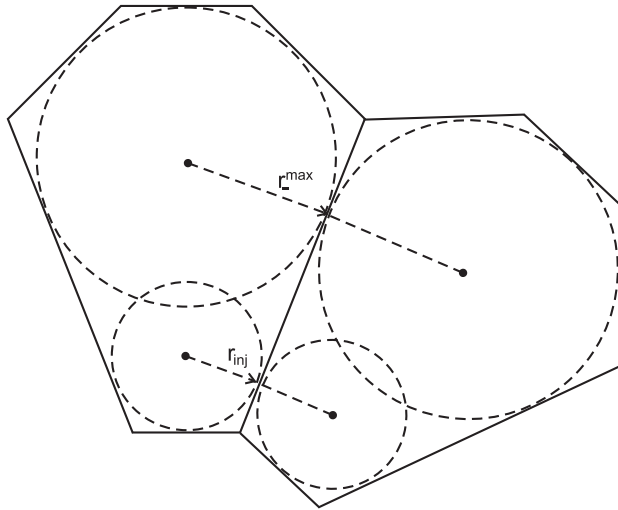


**FIGURE 2.** A schematic representation of two fundamental cells, and the indication of the injectivity radius  $r_{inj}$ , which is the radius of the smallest sphere ‘inscribable’ in the fundamental domain. The radius of the largest sphere ‘inscribable’  $r^{max}$  is also shown.

Now, for a given survey depth  $\chi_{obs}$  a topology is said to be undetectable if  $\chi_{obs} < r_{inj}$ . In this case no multiple images (or pattern repetitions of CMBR spots) can be detected in the survey of depth  $\chi_{obs}$ . On the other hand, when  $\chi_{obs} > r_{inj}$ , then the topology is detectable in principle or potentially detectable.

In a globally homogeneous manifold the above detectability condition holds regardless of the observer's position, and so if the topology is potentially detectable (or is undetectable) by an observer at  $x \in M$ , it is potentially detectable (or is undetectable) by an observer at any other point in the 3-space  $M$ . However, in globally inhomogeneous manifolds the detectability of cosmic topology depends on both the observer's position  $x$  and the survey depth  $\chi_{obs}$ . Nevertheless, even for globally inhomogeneous manifolds the above defined 'global' injectivity radius  $r_{inj}$  can be used to state an *absolute undetectability* condition, namely  $r_{inj} > \chi_{obs}$ , in the sense that if this condition holds the topology is undetectable for any observer at any point in  $M$ . Reciprocally, the condition  $\chi_{obs} > r_{inj}$  allows potential detectability (or detectability in principle) in the sense that, if this condition holds, multiple images of topological origin are potentially observable at least for some observers suitably located in  $M$ . An important point is that for spherical and hyperbolic manifolds, the 'global' injectivity radius  $r_{inj}$  expressed in terms of the curvature radius, is a constant (topological invariant) for a given topology.

Before proceeding further we shall recall some relevant results about spherical and hyperbolic 3-manifolds, which will be used to illustrate the above detectability condition. The multiply connected spherical 3-manifolds are of the form  $M = \mathbb{S}^3/\Gamma$ , where  $\Gamma$  is a finite subgroup of  $SO(4)$  acting freely on the 3-sphere. These manifolds were originally classified by Threlfall and Seifert [21], and are also discussed by Wolf [22] (for a description in the context of cosmic topology see [23]). Such a classification consists essentially in the enumeration of all finite groups  $\Gamma \subset SO(4)$ , and then in grouping the possible manifolds in classes. In a recent paper, Gausmann *et al.* [24] recast the classification in terms of single action, double action, and linked action manifolds. In table 1 we list the single action manifolds together with the symbol often used to refer to them, as well as the order of the covering group  $\Gamma$  and the corresponding injectivity radius. It is known that single action manifolds are globally homogeneous, and thus the detectability conditions for an observer at an arbitrary point  $p \in M$  also hold for an observer at any other point  $q \in M$ . Finally we note that the binary icosahedral group  $I^*$  gives the known Poincaré dodecahedral space, whose fundamental polyhedron is a regular spherical dodecahedron, 120 of which tile the 3-sphere into identical cells which are copies of the FP.

**TABLE 1.** Single action spherical manifolds together with the order of the covering group and the injectivity radius.

Name & Symbol	Order of $\Gamma$	Injectivity Radius
Cyclic $Z_n$	$n$	$\pi/n$
Binary dihedral $D_m^*$	$4m$	$\pi/2m$
Binary tetrahedral $T^*$	24	$\pi/6$
Binary octahedral $O^*$	48	$\pi/8$
Binary icosahedral $I^*$	120	$\pi/10$

Despite the enormous advances made in the last few decades, there is at present no complete classification of hyperbolic 3-manifolds. However, a number of important results have been obtained, including the two important theorems of Mostow [25] and Thurston [26]. According to the former, geometrical quantities of orientable hyperbolic manifolds, such as their volumes and the lengths of their closed geodesics, are topological invariants. Therefore quantities such as the 'global' injectivity radius  $r_{inj}$  (expressed in units of the curvature radius) are fixed for each manifold. Clearly this property also holds for spherical manifolds.

According to Thurston's theorem, there is a countable infinity of sequences of compact orientable hyperbolic manifolds, with the manifolds of each sequence being ordered in terms of their volumes. Moreover, each sequence has as an accumulation point a cusped manifold, which has finite volume, is non-compact, and has infinitely long cusped corners [26].

Closed orientable hyperbolic 3-manifolds can be constructed from these cusped manifolds. The compact manifolds are obtained through a so-called Dehn surgery which is a formal procedure identified by two coprime integers, i.e. winding numbers  $(n_1, n_2)$ . These manifolds can be constructed and studied with the publicly available software package SnapPea [27]. SnapPea names manifolds according to the seed cusped manifold and the winding numbers. So, for example, the smallest volume hyperbolic manifold known to date (Weeks' manifold) is named as m003(-3, 1), where m003 corresponds to a seed cusped manifold, and (-3, 1) is a pair of winding numbers. Hodgson and Weeks [27, 28] have compiled a census containing 11031 orientable closed hyperbolic 3-manifolds ordered by increasing volumes. In table 2 we collect the first ten manifolds from this census with the lowest volumes, ordered by increasing injectivity radius  $r_{inj}$ , together with their volumes.

**TABLE 2.** First seven manifolds in the Hodgson-Weeks census of closed hyperbolic manifolds, ordered by the injectivity radius  $r_{inj}$ , together with their corresponding volume.

Manifold	Injectivity Radius	Volume
m003(-4,1)	0.177	1.424
m004(3,2)	0.181	1.441
m003(-3,4)	0.182	1.415
m004(1,2)	0.183	1.398
m004(6,1)	0.240	1.284
m003(-4,3)	0.287	1.264
m003(-2,3)	0.289	0.981
m003(-3,1)	0.292	0.943
m009(4,1)	0.397	1.414
m007(3,1)	0.416	1.015

To illustrate now the above condition for detectability (undetectability) of cosmic topology, in the light of recent observations [9] we assume that the matter content of the universe is well approximated by dust of density  $\rho_m$  plus a cosmological constant  $\Lambda$ . In this cosmological setting the current curvature radius  $a_0$  of the spatial section is related to the total density parameter  $\Omega_0$  through the equation

$$a_0^2 = \frac{k}{H_0^2(\Omega_0 - 1)}, \quad (2)$$

where  $H_0$  is the Hubble constant,  $k$  is the normalized spatial curvature of the RW metric (1), and where here and in what follow the subscript 0 denotes evaluation at present time  $t_0$ . Furthermore, in this context the redshift-distance relation in units of the curvature radius,  $a_0 = R(t_0)$ , reduces to

$$\chi(z) = \sqrt{|1 - \Omega_0|} \int_1^{1+z} \frac{dx}{\sqrt{x^3 \Omega_{m0} + x^2(1 - \Omega_0) + \Omega_{\Lambda 0}}}, \quad (3)$$

where  $\Omega_{m0}$  and  $\Omega_{\Lambda 0}$  are, respectively, the matter and the cosmological density parameters, and  $\Omega_0 \equiv \Omega_{m0} + \Omega_{\Lambda 0}$ . For simplicity, on the left hand side of (3) and in many places of this article, we have left implicit the dependence of the function  $\chi$  on the density components.

A first qualitative estimate of the constraints on detectability of cosmic topology from nearflatness can be obtained from the function  $\chi(\Omega_{m0}, \Omega_{\Lambda 0}, z)$  given by (3) for a fixed survey depth  $z$ . Figure 3 clearly demonstrates the rapid way  $\chi$  drops to zero in a narrow neighbourhood of the  $\Omega_0 = 1$  line. This can be understood intuitively from (2), since the natural unit of length (the curvature radius  $a_0$ ) goes to infinity as  $\Omega_0 \rightarrow 1$ , and therefore the depth  $\chi$  (for any fixed  $z$ ) of the observable universe becomes smaller in this limit. From the observational point of view, this shows that the detection of the topology of the nearly flat universes becomes more and more difficult as  $\Omega_0 \rightarrow 1$ , a limiting value favoured by recent observations. As a consequence, by using any method which relies on observations of repeated patterns the topology of an increasing number of nearly flat universes becomes undetectable in the light of the recent observations, which indicate that  $\Omega_0 \sim 1$ .

From the above discussion it is clear that cosmic topology may be undetectable for a given survey up to a depth  $z_{max}$ , but detectable if one uses a deeper survey. At present the deepest survey available corresponds to  $z_{max} = z_{LSS} \sim 1000$ , with associated depth  $\chi(z_{LSS})$ . So the most promising searches for cosmic topology through multiple images of radiating sources are based on CMBR.

As a concrete quantitatively example we consider universes with that possess a cyclic single action spherical topologies for  $\Omega_0 = 1.08$  and  $\Omega_{\Lambda} = 0.66$ . From table 1 we have  $r_{inj} = \pi/n$  which together with the undetectability condition give

$$\chi_{obs} < r_{inj} \implies n < n^* = \text{int} \left( \frac{\pi}{\chi_{obs}} \right), \quad (4)$$

where  $\text{int}(x)$  denotes the integer part of  $x$ .

In table 3 for distinct redshifts  $z_{max}$  we collect the corresponding survey depth  $\chi_{obs}$  and the limiting value below which the cyclic single action manifold is undetectable. According to this table the cyclic group manifolds  $\mathbb{Z}_2$  and  $\mathbb{Z}_3$

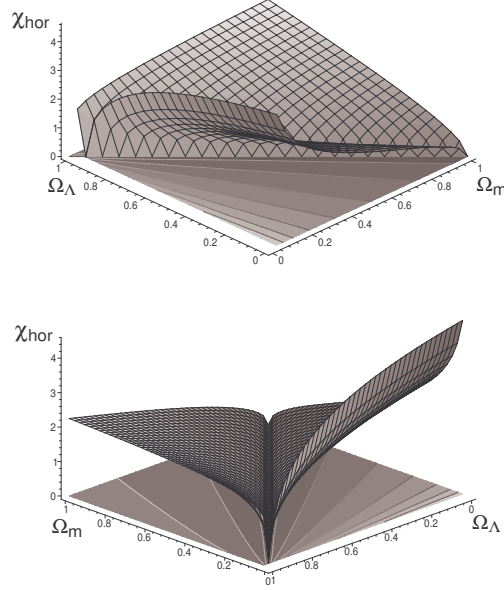


**FIGURE 3.** The behaviour of  $\chi_{hor} = \chi(\Omega_{m0}, \Omega_{\Lambda0}, z)$ , in units of curvature radius, for  $z = 1100$  as a function of the density parameters  $\Omega_{\Lambda0}$  and  $\Omega_{m0}$ . These figures show clearly the rapid way  $\chi_{hor}$  falls off to zero for nearly flat (hyperbolic or elliptic) universes

are undetectable even if one uses CMBR, while the manifolds  $S^3/\mathbb{Z}_p$  for  $p \geq 4$  are detectable with CMBR. For the same values of the density parameters (besides  $\mathbb{Z}_2$  and  $\mathbb{Z}_3$  manifolds) the manifolds  $\mathbb{Z}_4$ ,  $\mathbb{Z}_5$  and  $\mathbb{Z}_6$  are undetectable using sources of redshifts up to  $z_{max} = 6$ .

**TABLE 3.** For each  $z_{max}$  the corresponding values  $\chi_{obs}$  for  $\Omega_0 = 1.08$  and  $\Omega_{\Lambda} = 0.66$ . The integer number  $n^*$  is the limiting value below which the corresponding cyclic topology is undetectable.

Redshift $z_{max}$	Depth $\chi_{obs}$	Limiting value $n^*$
1100	0.811	4
6	0.496	7
1	0.209	16

To quantitatively illustrate the above features of the detectability problem in the hyperbolic case ( $\Omega_0 < 1$ ), we shall examine the detectability of cosmic topology of the first ten smallest (volume) hyperbolic universes. To this end we shall take the following interval of the density parameters values consistent with current observations:  $\Omega_0 \in [0.99, 1)$  and  $\Omega_{\Lambda0} \in [0.63, 0.73]$ . In this hyperbolic sub-interval one can calculate the largest value of  $\chi_{obs}(\Omega_{m0}, \Omega_{\Lambda0}, z)$  for the last scattering surface ( $z = 1100$ ), and compare with the injectivity radii  $r_{inj}$  to decide upon detectability. From (3) one obtains  $\chi_{obs}^{max} = 0.337$ .

Table 4 summarizes the results for CMBR ( $z = 1100$ ), which have been refined upon by Weeks [19]. It makes explicit the very important fact that there are undetectable topologies by any methods that rely on pattern repetitions even if one uses CMBR, which corresponds to the deepest survey depth  $\chi(z_{LSS})$ .

Hitherto we have considered the detectability of nearly flat universe, but one can alternatively ask what is the region of the density parameter spaces for which topologies are detectable. To this end, we note that for a given (fixed) survey with redshift cut-off  $z_{obs}$ , and for a given manifold with injectivity radius  $r_{inj}^M$  one can solve the equation

$$\chi(\Omega_0, \Omega_{\Lambda}, z_{obs}) = r_{inj}^M, \quad (5)$$

which amounts to finding pairs  $(\Omega_0, \Omega_{\Lambda0})$  in the density parameter  $\Omega_0 - \Omega_{\Lambda0}$  plane for which eq. (5) holds.<sup>2</sup>

<sup>2</sup> Since  $\Omega_0 = \Omega_{m0} + \Omega_{\Lambda0}$  we can clearly take  $\chi$  as function of either  $(\Omega_0, \Omega_{m0})$  or  $(\Omega_{m0}, \Omega_{\Lambda0})$ .

**TABLE 4.** Restrictions on detectability of cosmic topology for  $\Omega_0=0.99$  with  $\Omega_{\Lambda 0} \in [0.63, 0.73]$  for the first ten smallest known hyperbolic manifolds. A survey depth corresponding to CMBR ( $z_{max} = 1100$ ) was used. The manifolds are ordered by increasing volumes.

Manifold	Volume	Injectivity radius	Detectability with CMBR
m003(-3,1)	0.943	0.292	Potential Detectable
m003(-2,3)	0.981	0.289	Potential Detectable
m007(3,1)	1.015	0.416	Undetectable
m003(-4,3)	1.264	0.287	Potential Detectable
m004(6,1)	1.284	0.240	Potential Detectable
m004(1,2)	1.398	0.183	Potential Detectable
m009(4,1)	1.414	0.397	Undetectable
m003(-3,4)	1.415	0.182	Potential Detectable
m003(-4,1)	1.424	0.177	Potential Detectable
m004(3,2)	1.441	0.181	Potential Detectable

Consider now the set of the 19 smallest manifolds of the Hodgson-Weeks census in conjunction with the hyperbolic region

$$\Omega_0 \in [0.98, 1) \quad \text{and} \quad \Omega_{\Lambda 0} \in [0.62, 0.79], \quad (6)$$

and the eqs. (3) and (5). The manifold in this set with the lowest  $r_{inj}$  ( $= 0.152$ ) is  $m003(-5, 4)$  (see [27]). Figure 4 gives the solution curve of equation (5) in the  $\Omega_0 - \Omega_{\Lambda 0}$  plane for  $r_{inj} = 0.152$  and  $r_{inj} = 0.081$ , where a survey of depth  $z_{max} = 1100$  (CMBR) was used. This figure also contains a dashed rectangular box, representing the relevant part of the recent hyperbolic region (6). For each value of  $r_{inj}$  undetectability is ensured for the values of cosmological

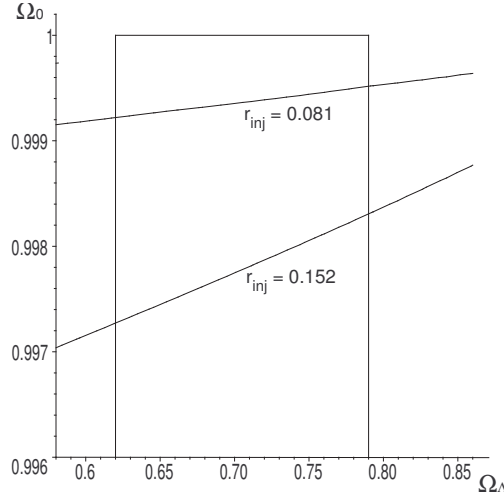


**FIGURE 4.** The solution curves of  $\chi_{obs}(\Omega_0, \Omega_{\Lambda 0}, z) = r_{inj}$ , as plots of  $\Omega_0$  versus  $\Omega_{\Lambda 0}$  for  $r_{inj} = 0.081$  and  $r_{inj} = 0.152$ . A survey with depth  $z_{max} = 1100$  (CMBR) was used. The dashed rectangular box represents the relevant part of the hyperbolic region (6) of the parameter space given by recent observations. The undetectable regions of the parameter space  $(\Omega_0, \Omega_{\Lambda 0})$ , corresponding to each value of  $r_{inj}$ , lie above the related curve.

parameters (region in the  $\Omega_0 - \Omega_{\Lambda 0}$  plane) which lie above the corresponding solution curve of (5). Thus, considering the solution curve of (5) for  $r_{inj} = 0.152$ , for example, one finds that the topology of none of the 19 smallest manifolds of the census would be detectable, if  $\Omega_0 \gtrsim 0.9971$ . On the other hand, one has that this value is a lower bound for the total density parameter  $\Omega_0$  if it turns out that one of these 19 hyperbolic manifolds is detected.

For a given survey with redshift cut-off  $z_{obs}$ , the redshift distance function  $\chi_{obs}$  clearly depends on the way one models the matter-energy content of the universe. This point has been recently discussed by Mota *et al.* in a unifying dark matter and dark energy framework [13].

In what follows we shall briefly discuss two important results related to detectability of cosmic topology. For more details we refer the readers to refs. [11] and [12]. Regarding the first, consider again the solution curve of (5) in the

parameter plane. For a given survey depth  $z_{obs}$  we define the secant line as the line joining the points  $(\tilde{\Omega}_{m0}, 0)$  and  $(0, \tilde{\Omega}_{\Lambda0})$  where the contour curve intersects the axes  $\Omega_{m0}$  and  $\Omega_{\Lambda0}$ , respectively. Clearly the equation of this line is given by

$$\frac{\Omega_{m0}}{\tilde{\Omega}_{m0}} + \frac{\Omega_{\Lambda0}}{\tilde{\Omega}_{\Lambda0}} = 1. \quad (7)$$

It is possible to show that the solution curve of (5) is convex and concave, respectively, in the hyperbolic and spherical regions of the parameter plane  $\Omega_{\Lambda0} - \Omega_{m0}$ . This property can also be gleaned from the parametric plot of the solution curve of (5), and ensures that the secant line crosses the contour line only at the  $\Omega_{m0}$  and  $\Omega_{\Lambda0}$  axes. As a consequence the region between the secant line and the flat line  $\Omega_{\Lambda0} + \Omega_{m0} = 1$  lies inside the undetectability region of the parameter plane. Thus, the secant line approximation to the solution curve of (5) gives a sufficient condition for undetectability of the corresponding topology with injectivity radius  $r_{inj}^M$ . A closed form for this sufficient condition can be obtained from (7) in the limiting case  $z \rightarrow \infty$ . As a result one has that a universe with space section M has undetectable topology if

$$\begin{aligned} \cosh^2(r_{inj}^M/2) \Omega_{m0} + \Omega_{\Lambda0} &> 1, \quad \text{for } \Omega_0 < 1, \\ \cos^2(r_{inj}^M/2) \Omega_{m0} + \Omega_{\Lambda0} &< 1, \quad \text{for } \Omega_0 > 1. \end{aligned} \quad (8)$$

Despite its simple form, this result is of considerable interest in that it gives a test for undetectability for *any*  $z$ .

The condition (8) can easily be written in terms of either  $\Omega_0$  and  $\Omega_{\Lambda0}$  or  $\Omega_0$  and  $\Omega_{m0}$  [11]. So, for example, a universe space section M has undetectable topology if

$$\begin{aligned} \Omega_0 &> 1 - \sinh^2(r_{inj}^M/2) \Omega_{m0}, \quad \text{for } \Omega_0 < 1, \\ \Omega_0 &< 1 + \sin^2(r_{inj}^M/2) \Omega_{m0}, \quad \text{for } \Omega_0 > 1. \end{aligned} \quad (9)$$

From table 1 we have the injectivity radius for the single action cyclic  $\mathbb{Z}_n$  and binary dihedral  $D_m^*$  families are given, respectively, by  $r_{inj} = \pi/n$  and  $r_{inj} = \pi/2m$ . This allows to solve the equation corresponding to (9) to obtain

$$\begin{aligned} n^* &= \text{int} \left\{ \frac{\pi}{2} \left[ \arcsin \sqrt{\frac{\Omega_0 - 1}{\Omega_{m0}}} \right]^{-1} \right\}, \\ m^* &= \text{int} \left\{ \frac{\pi}{4} \left[ \arcsin \sqrt{\frac{\Omega_0 - 1}{\Omega_{m0}}} \right]^{-1} \right\}, \end{aligned} \quad (10)$$

where  $\text{int}[x]$  denotes the integer part of  $x$ . Thus, for these two classes of manifold there is always  $n^*$  and  $m^*$  such that the corresponding topology is detectable for  $n > n^*$  and  $m > m^*$ , given in terms of the density parameters.

The second important result is related to detectability of very nearly flat universes, for which  $|\Omega_0 - 1| \ll 1$  [12]. If in addition to this condition we make two further physically motivated assumptions: (i) the observer is at a position  $x$  where the topology is detectable, i.e.  $r_{inj}(x) < \chi_{obs}$ ; and (ii) the topology is not excludable, i.e. it does not produce too many images so as to be ruled out by present observations. Thus, these main physical assumption can be summarized as

$$r_{inj}(x) \lesssim \chi_{obs} \ll 1. \quad (11)$$

These assumptions severely restricts the set of detectable nearly flat manifolds. Thus in the case of spherical manifolds, only cyclic ( $r_{inj} = \pi/n$ ) and binary dihedral spaces ( $r_{inj} = \pi/2m$ ) of sufficiently high order of  $n$  or  $4m$  are detectable. In the hyperbolic case, the only detectable manifolds are the so-called nearly cusped manifolds, which are sufficiently similar to the cusped manifolds (cusped manifolds are non-compact, and possess regions with arbitrarily small  $r_{inj}(x)$ .)

In a recent study [12] we considered both classes of manifolds and showed that a generic detectable spherical or hyperbolic manifold is locally indistinguishable from either a cylindrical ( $\mathbb{R}^2 \times \mathbb{S}^1$ ) or toroidal ( $\mathbb{R} \times \mathbb{T}^2$ ) manifold, irrespective of its global shape. These results have important consequences in the development of search strategies for cosmic topology. They show that for a typical observer in a very nearly flat universe, the 'detectable part' of the topology would be indistinguishable from either  $\mathbb{R}^2 \times \mathbb{S}^1$  or  $\mathbb{R} \times \mathbb{T}^2$  manifold.

To conclude this section, we mention that Makler *et al.* have examined, in a recent article [14], the extent to what a possible detection of a non-trivial topology of a low curvature ( $\Omega_0 \sim 1$ ) universe may be used to place constraints



on the matter content of the universe, focusing our attention on the generalized Chaplygin gas (GCG) model, which unifies dark matter and dark energy in a single matter component. It is shown that besides constraining the GCG parameters, the detection of a nontrivial topology also allows to set bounds on the total density parameter  $\Omega_0$ . It is also studied the combination of the bounds from the topology detection with the limits that arise from current data on SNIa, and shown that the detection of a nontrivial topology sets complementary bounds on the GCG parameters (and on  $\Omega_0$ ) to those obtained from the SNIa data alone (for examples of local physical effect of a possible nontrivial topology see, e.g., refs. [15] – [?]).

#### 4. PAIR SEPARATIONS STATISTICAL METHODS

On the one hand the most fundamental consequence of a multiply connected spatial section  $M$  for the universe is the existence of multiple images of cosmic sources, on the other hand a number of observational problems render the direct identification of these images practically impossible. In the statistical approaches to detect the cosmic topology instead of focusing on the direct recognition of multiple images, one treats statistically the images of a given cosmic source, and use (statistical) indicators or signatures in the search for a sign of a nontrivial topology. Hence the statistical methods are not plagued by direct recognition difficulties such as morphological effects, and distinct stages of the evolution of cosmic sources.

The key point of these methods is that in a universe with detectable nontrivial topology at least one of the characteristic sizes of the space section  $M$  is smaller than a given survey depth  $\chi_{obs}$ , so the sky should show multiple images of sources, whose 3-D positions are correlated by the isometries of the covering group  $\Gamma$ . These methods rely on the fact that the correlations among the positions of these images can be couched in terms of distance correlations between the images, and use statistical indicators to find out signs of a possible nontrivial topology of  $M$ .

In 1996 Lehoucq *et al.* [29] proposed the first statistical method (often referred to as cosmic crystallography), which looks for these correlations by using pair separations histograms (PSH). To build a PSH we simply evaluate a suitable one-to-one function  $F$  of the distance  $d$  between a pair of images in a catalogue  $\mathcal{C}$ , and define  $F(d)$  as the pair separation:  $s = F(d)$ . Then we depict the number of pairs whose separation lie within certain sub-intervals  $J_i$  partitions of  $(0, s_{max}]$ , where  $s_{max} = F(2\chi_{max})$ , and  $\chi_{max}$  is the survey depth of  $\mathcal{C}$ . A PSH is just a normalized plot of this counting. In most applications in the literature the separation is taken to be simply the distance between the pair  $s = d$  or its square  $s = d^2$ ,  $J_i$  being, respectively, a partition of  $(0, 2\chi_{max}]$  and  $(0, 4\chi_{max}^2]$ .

The PSH building procedure can be formalized as follows. Consider a catalogue  $\mathcal{C}$  with  $n$  cosmic sources and denote by  $\eta(s)$  the number of pairs of sources whose separation is  $s$ . Divide the interval  $(0, s_{max}]$  in  $m$  equal sub-intervals (bins) of length  $\delta s = s_{max}/m$ , being

$$J_i = (s_i - \frac{\delta s}{2}, s_i + \frac{\delta s}{2}], ; \quad i = 1, 2, \dots, m ,$$

and centered at  $s_i = (i - \frac{1}{2}) \delta s$ . The PSH is defined as the following counting function:

$$\Phi(s_i) = \frac{2}{n(n-1)} \frac{1}{\delta s} \sum_{s \in J_i} \eta(s) , \quad (12)$$

which can be seen to be subject to the normalization condition  $\sum_{i=1}^m \Phi(s_i) \delta s = 1$ . An important advantage of using *normalized* PSH's is that one can compare histograms built up from catalogues with different number of sources.

An example of PSH obtained through simulation for a universe with nontrivial topology is given in Fig. 5. Two important features should be noticed: (i) the presence of the very sharp peaks (called spikes); and (ii) the existence of a 'mean curve' above which the spikes stands. This curve corresponds to an expected pair separation histogram (EPSH)  $\Phi_{exp}(s_i)$ , which is a typical PSH from which the statistical noise has been withdrawn, that is  $\Phi_{exp}(s_i) = \Phi(s_i) - \rho(s_i)$ , where  $\rho(s_i)$  represents the statistical fluctuation that arises in the PSH  $\Phi(s_i)$ .

The primary expectation was that the distance correlations would manifest as topological spikes in PSH's, and that the spike spectrum of topological origin would be a definite signature of the topology [29]. While the first simulations carried out for specific flat manifolds appeared to confirm this expectation [29], histograms subsequently generated for specific hyperbolic manifolds revealed that the corresponding PSH's exhibit no spikes [30, 31]. Concomitantly, a theoretical statistical analysis of the distance correlations in PSH's was accomplished, and a proof was presented that the spikes of topological origin in PSH's are due to just one type of isometry: the Clifford translations (CT) [32], which are isometries  $g_t \in \Gamma$  such that for all  $p \in \tilde{M}$  the distance  $d(p, g_t p)$  is a constant (see also in this regard [30]). Clearly

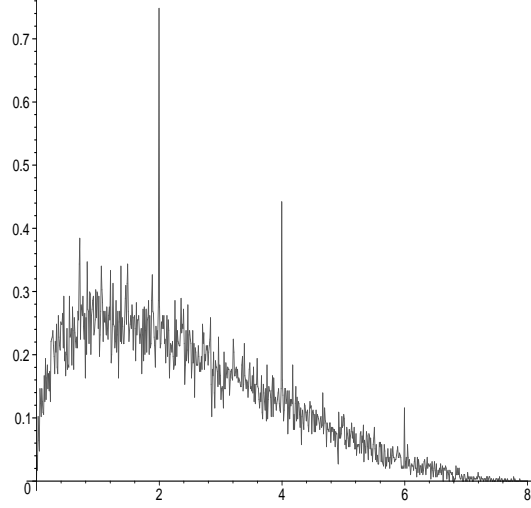


**FIGURE 5.** Typical PSH for a flat universe with a 3–torus topology. The horizontal axis gives the squared pair separation  $s^2$ , while the vertical axis provides a normalized number of pairs.

the CT's reduce to the regular translations in the Euclidean spaces (for more details and simulations see [33] – [35]). Since there is no CT translation in hyperbolic geometry this result explains the absence of spikes in the PSH's of hyperbolic universes with nontrivial detectable topology. On the other hand, it also makes clear that distinct manifolds which admit the same Clifford translations in their covering groups present the same spike spectrum of topological origin. Therefore the topological spikes are not sufficient for unambiguously determine the topology of the universe.

In spite of these limitations, the most striking evidence of multiply-connectedness in PSH's is indeed the presence of topological spikes, which result from translational isometries  $g_t \in \Gamma$ . It was demonstrated [32, 33] that the other isometries  $g$  manifest as very tiny deformations of the expected pair separation histogram  $\Phi_{exp}^{sc}(s_i)$  corresponding to the underlying simply connected universe [36, 37]. Furthermore, in PSH's of universes with nontrivial topology the amplitude of the sign of non-translational isometries was shown to be smaller than the statistical noise [33], making clear that one cannot use PSH to reveal these isometries.

In brief, the only significant (measurable) sign of a nontrivial topology in PSH are the spikes, but they can be used merely to disclose (not to determine) a possible nontrivial topology of universes that admit Clifford translations: any flat, some spherical, and no hyperbolic universes.

The impossibility of using the PSH method for the detection of the topology of hyperbolic universes motivated the development of a new scheme called *collecting correlated pairs method* (CCP method) [38] to search for cosmic topology.

In the CCP method it is used the basic feature of the isometries, i.e., that they preserve the distances between pairs of images. Thus, if  $(p, q)$  is a pair of arbitrary images (correlated or not) in a given catalogue  $\mathcal{C}$ , then for each  $g \in \Gamma$  such that the pair  $(gp, gq)$  is also in  $\mathcal{C}$  we obviously have

$$d(p, q) = d(gp, gq) . \quad (13)$$

This means that for a given (arbitrary) pair  $(p, q)$  of images in  $\mathcal{C}$ , if there are  $n$  isometries  $g \in \Gamma$  such that both images  $gp$  and  $gq$  are still in  $\mathcal{C}$ , then the separation  $s(p, q)$  will occur  $n$  times.

The easiest way to understand the CCP method is by looking into its computer-aided procedure steps, and then examine the consequences of having a multiply connected universe with detectable topology. To this end, let  $\mathcal{C}$  be a catalogue with  $n$  sources, so that one has  $P = n(n - 1)/2$  pairs of sources. The CCP procedure consists on the following steps:

1. Compute the  $P$  separations  $s(p, q)$ , where  $p$  and  $q$  are two images in the catalogue  $\mathcal{C}$ ;
2. Order the  $P$  separations in a list  $\{s_i\}_{1 \leq i \leq P}$  such that  $s_i \leq s_{i+1}$ ;
3. Create a list of *increments*  $\{\Delta_i\}_{1 \leq i \leq P-1}$ , where  $\Delta_i = s_{i+1} - s_i$ ;

4. Define the CCP index as

$$\mathcal{R} = \frac{\mathcal{N}}{P-1},$$

where  $\mathcal{N} = \text{Card}\{i : \Delta_i = 0\}$  is the number of times the increment is null.

If the smallest characteristic length of  $M$  exceeds the survey depth ( $r_{inj} > \chi_{obs}$ ) the probability that two pairs of images are separated by the same distance is zero, so  $\mathcal{R} \approx 0$ . On the other hand, in a universe with detectable nontrivial topology ( $\chi_{obs} > r_{inj}$ ) given  $g \in \Gamma$ , if  $p$  and  $q$  as well as  $gp$  and  $gq$  are images in  $\mathcal{C}$ , then: (i) the pairs  $(p, q)$  and  $(gp, gq)$  are separated by the same distance; and (ii) when  $\Gamma$  admits a translation  $g_t$  the pairs  $(p, g_t p)$  and  $(q, g_t q)$  are also separated by the same distance. It follows that when a nontrivial topology is detectable, and a given catalogue  $\mathcal{C}$  contains multiple images, then  $\mathcal{R} > 0$ , so the CCP index is an indicator of a detectable nontrivial topology of the spatial section  $M$  of the universe. Note that although  $\mathcal{R} > 0$  can be used as a sign of multiply connectedness, it gives no indication as to what the actual topology of  $M$  is. Clearly whether one can find out that  $M$  is multiply connected (compact in at least one direction) is undoubtedly a very important step, though.

In more realistic situations, uncertainties in the determination of positions and separations of images of cosmic sources are dealt with through the following extension of the CCP index: [38]

$$\mathcal{R}_\varepsilon = \frac{\mathcal{N}_\varepsilon}{P-1},$$

where  $\mathcal{N}_\varepsilon = \text{Card}\{i : \Delta_i \leq \varepsilon\}$ , and  $\varepsilon > 0$  is a parameter that quantifies the uncertainties in the determination of the pairs separations.

Both PSH and CCP statistical methods rely on the accurate knowledge of the three-dimensional positions of the cosmic sources. The determination of these positions, however, involves inevitable uncertainties, which basically arises from: (i) uncertainties in the determination of the values of the cosmological density parameters  $\Omega_{m0}$  and  $\Omega_{\Lambda0}$ ; (ii) uncertainties in the determination of both the red-shifts (due to spectroscopic limitations), and the angular positions of cosmic objects (displacement, due to gravitational lensing by large scale objects, e.g.); and (iii) uncertainties due to the peculiar velocities of cosmic sources, which introduce peculiar red-shift corrections. Furthermore, in most studies related to these methods the catalogues are taken to be complete, but real catalogues are incomplete: objects are missing due to selection rules, and also most surveys are not full sky coverage surveys. Another very important point to be considered regarding these statistical methods is that most of cosmic objects do not have very long lifetimes, so there may not even exist images of a given source at large red-shift. This poses the important problem of what is the suitable source (candle) to be used in these methods.

Some of the above uncertainties, problems and limits of the statistical methods have been discussed by Lehoucq *et al.* [39], but the robustness of these methods still deserves further investigation. So, for example, a quantitative study of the sensitivity of spikes and CCP index with respect to the uncertainties in the positions of the cosmic sources, which arise from unavoidable uncertainties in values of the density parameters is being carried out [40].

For completeness we mention the recent articles by Marecki *et al.* [41], and by Bernui *et al.* [42]. Bernui and Villela have worked with a method which uses pair angular separation histograms (PASH) in connection with both discrete cosmic sources and CMBR.

To close this section we refer the reader to references [43, 44], which present alternative statistical methods (see also the review articles [45]).

## 5. LOOKING FOR THE TOPOLOGY USING CMBR

The CMB temperature anisotropy measurements by WMAP combine high angular resolution, and high sensitivity, with the full sky and the deepest survey ( $z_{LSS} \sim 1100$ ) currently available. These features make very promising the observational probe of cosmic topology with CMBR anisotropies on length scales near to or even somewhat beyond the horizon  $\chi_{hor}$ .

Over the past few years distinct approaches to probe a non-trivial topology of the universe using CMBR have been suggested. In a recent paper Souradeep and Hajian [46, 47] have grouped these approaches in three broad families. Here, however, we shall briefly focus on the most well known method that relies on multiple images of spots in the CMBR maps, which is known as circles-in-the-sky [48] (for more detail on the other methods see, e.g., refs. [49] – [56]).

For an observer in the Hubble flow the last scattering surface (LSS) is well approximated by a two-sphere of radius  $\chi_{LSS}$ . If a non-trivial topology of space is detectable, then this sphere intersects some of its topological images, giving rise to circles-in-the-sky, i.e., pairs of matching circles of equal radii, centered at different points on the LSS sphere, with the same pattern of temperature variations [48]. These matched circles will exist in CMBR anisotropy maps of universes with any detectable nontrivial topology, regardless of its geometry.

The mapping from the last scattering surface to the sky sphere is conformal. Since conformal maps preserve angles, the identified circle at the LSS would appear as identified circles on the sky sphere. A pair of matched circles is described as a point in a six-dimensional parameter space. These parameters are the centers of each circle, which are two points on the unit sphere (four parameters), the angular radius of both circles (one parameter), and the relative phase between them (one parameter).

Pairs of matched circles may be hidden in the CMBR maps if the universe has a detectable topology. Therefore to observationally probe nontrivial topology on the available largest scale, one needs a statistical approach to scan all-sky CMBR maps in order to draw the correlated circles out of them.<sup>3</sup> To this end, let  $\mathbf{n}_1 = (\theta_1, \varphi_1)$  and  $\mathbf{n}_2 = (\theta_2, \varphi_2)$  be the center of two circles  $C_1$  and  $C_2$  with angular radius  $\rho$ . The search for the matching circles can be performed by computing the following correlation function [48]:

$$S(\alpha) = \frac{\langle 2T_1(\pm\phi)T_2(\phi + \alpha) \rangle}{\langle T_1(\pm\phi)^2 + T_2(\phi + \alpha)^2 \rangle}, \quad (14)$$

where  $T_1$  and  $T_2$  are the temperature anisotropies along each circle,  $\alpha$  is the relative phase between the two circles, and the mean is taken over the circle parameter  $\phi$ :  $\langle \rangle = \int_0^{2\pi} d\phi$ . The plus (+) and minus (-) signs in (14) correspond to circles correlated, respectively, by non-orientable and orientable isometries.

For a pair of circles correlated by an isometry (perfectly matched) one has  $T_1(\pm\phi) = T_2(\phi + \alpha_*)$  for some  $\alpha_*$ , which gives  $S(\alpha_*) = 1$ , otherwise the circles are uncorrelated and so  $S(\alpha) \approx 0$ . Thus a peaked correlation function around some  $\alpha_*$  would mean that two matched circles, with centers at  $\mathbf{n}_1$  and  $\mathbf{n}_2$ , and angular radius  $\rho$ , have been detected.

From the above discussion it is clear that a full search for matched circles requires the computation of  $S(\alpha)$ , for any permitted  $\alpha$ , sweeping the parameter sub-space  $(\theta_1, \varphi_1, \theta_2, \varphi_2, \rho)$ , and so it is indeed computationally very expensive. Nevertheless, such a search is currently in progress, and preliminary results using the first year WMAP data failed to find antipodal and nearly antipodal, matched circles with radii larger than  $25^\circ$  [58]. Here nearly antipodal means circles whose centers are separated by more than  $170^\circ$ . At a first sight this preliminary result seems to rule out topologies whose isometries produce antipodal images of the observer, as for example the Poincaré dodecahedron model [59], or any other homogeneous spherical space with detectable isometries. In this regard, it is important to note the results of the recent articles by Roukema *et al.* [60] and Aurich *et al.* [61], Gundermann [62], and some remarks by Luminet [63], which support the dodecahedron model.

Furthermore, since detectable topologies (isometries) do not produce, in general, antipodal correlated circles, a little more can be inferred from the lack of nearly antipodal matched circles. Thus, in a flat universe, e.g., any screw motion may generate pairs of circles that are not even nearly antipodal, provided that the observer's position is far enough from the axis of rotation [64, 65]. As a consequence, our universe can still have a flat topology, other than the 3-torus, but in this case the axis of rotation of the screw motion corresponding to a pair of matched circles would pass far from our position, making clear the crucial importance of the position of the observer relative to the 'axis of rotation' in the matching circles search method.

## ACKNOWLEDGMENTS

I thank CNPq for the grant under which this work was carried out, and M. Novello for the invitation to give a set of lectures in the XI<sup>th</sup> Brazilian School of Cosmology and Gravitation. I also thank B. Mota for his valuable help in polishing the figures and for the reading of the manuscript and indication of misprints and omissions.

In my life, learning has often been a cooperative process in which contributions have come from many quarters consciously as well as unconsciously. I have learned a lot from my collaborators. Many warmest thanks go to them all.

---

<sup>3</sup> In practice, however, contributions such as integrated Sachs-Wolfe effect, the tickness of the last scattering surface, and even aberration effect [57] may damage or even destroy the matching of the circles.

## REFERENCES

1. C.L. Bennett et al. , *Astrophys. J.* **583**, 1 (2003);  
D.N. Spergel et al. , *Astrophys. J. Suppl.* **148**, 175 (2003);  
G. Hinshaw et al. , *Astrophys. J. Suppl.* **148**, 135 (2003);  
C.L. Bennett et al. , *Astrophys. J. Suppl.* **148**, 1 (2003).
2. D.D. Sokolov and V.F. Shvartsman, *Sov. Phys. JETP* **39**, 196 (1974).
3. L-Z. Fang and H. Sato, *Gen. Rel. Grav.* **17** 1117 (1985).
4. D.D. Sokolov and A.A. Starobinsky, *Sov. Astron.* **19**, 629 (1975).
5. J.R. Gott, *Mon. Not. R. Astron. Soc.* **193**, 153 (1980).
6. H.V. Fagundes, *Phys. Rev. Lett.* **51**, 417 (1983).
7. H.V. Fagundes and U.F. Wichoski, *Astrophys. J.* **322**, L52 (1987).
8. G.I. Gomero, *Class. Quantum Grav.* **20**, 4775 (2003).
9. M. Tegmark et al., *Phys. Rev. D* **69**, 103501 (2004).
10. G.I. Gomero and M.J. Rebouças, *Phys. Lett. A* **311**, 319 (2003);  
G.I. Gomero, M.J. Rebouças, and R. Tavakol, *Class. Quantum Grav.* **18**, 4461 (2001);  
G.I. Gomero, M.J. Rebouças, and R. Tavakol, *Class. Quantum Grav.* **18**, L145 (2001);  
G.I. Gomero, M.J. Rebouças, and R. Tavakol, *Int. J. Mod. Phys. A* **17**, 4261 (2002);  
B. Mota, M.J. Rebouças, and R. Tavakol, astro-ph/0403110;  
B. Mota, M.J. Rebouças, and R. Tavakol, astro-ph/0503683.
11. B. Mota, M.J. Rebouças, and R. Tavakol, *Class. Quantum Grav.* **20**, 4837 (2003).
12. B. Mota, G.I. Gomero, M.J. Rebouças, and R. Tavakol, *Class. Quantum Grav.* **21**, 3361 (2004).
13. M. Makler, B. Mota, and M.J. Rebouças, CBPF NF-030/04.
14. M. Makler, B. Mota, and M.J. Rebouças, submitted for publication (2005).
15. W. Oliveira, M.J. Rebouças, and A.F.F. Teixeira, *Phys. Lett. A* **188**, 125 (1994).
16. A. Bernui, G.I. Gomero, M.J. Rebouças, and A.F.F. Teixeira, *Phys. Rev. D* **57**, 4699 (1998).
17. M.J. Rebouças, R. Tavakol, and A.F.F. Teixeira, *Gen. Rel. Grav.* **30**, 535 (1998).
18. G.I. Gomero, M.J. Rebouças, A.F.F. Teixeira and A. Bernui, *Int. J. Mod. Phys. A* **15**, 4141 (2000).
19. J.R. Weeks, *Mod. Phys. Lett. A* **18**, 2099 (2003).
20. J. Weeks, R. Lehoucq, and J.-P. Uzan, *Class. Quant. Grav.* **20**, 1529 (2003).
21. W. Threlfall and H. Seifert, *Math. Annalen* **104**, 543 (1932).
22. J.A. Wolf, *Spaces of Constant Curvature*, fifth ed., Publish or Perish Inc., Delaware (1984).
23. G.F.R. Ellis, *Gen. Rel. Grav.* **2**, 7 (1971).
24. E. Gausmann, R. Lehoucq, J.-P. Luminet, J.-P. Uzan, and J. Weeks, *Class. Quant. Grav.* **18**, 5155 (2001).
25. G.D. Mostow, *Ann. Math. Studies* **78** (1973), Princeton University Press, Princeton, New Jersey.
26. W.P. Thurston, *Bull. Am. Math. Soc.* **6**, 357 (1982);  
W.P. Thurston, *Three-dimensional geometry and topology* (1997) Princeton Mathematical series **35**, Ed. S. Levy, (Princeton University Press, Princeton, USA).
27. J.R. Weeks, SnapPea: A computer program for creating and studying hyperbolic 3-manifolds, available at <http://geometrygames.org/SnapPea/>
28. C.D. Hodgson and J.R. Weeks, *Experimental Mathematics* **3**, 261 (1994).
29. R. Lehoucq, M. Lachièze-Rey, and J.-P. Luminet, *Astron. Astrophys.* **313**, 339 (1996).
30. R. Lehoucq, J.-P. Luminet, and J.-P. Uzan, *Astron. Astrophys.* **344**, 735 (1999).
31. H.V. Fagundes and E. Gausmann, astro-ph/9811368.
32. G.I. Gomero, A.F.F. Teixeira, M.J. Rebouças, and A. Bernui, *Int. J. Mod. Phys. D* **11**, 869 (2002). Also gr-qc/9811038.
33. G.I. Gomero, M.J. Rebouças, and A.F.F. Teixeira, *Phys. Lett. A* **275**, 355 (2000).
34. G.I. Gomero, M.J. Rebouças, and A.F.F. Teixeira, *Int. J. Mod. Phys. D* **9**, 687 (2000).
35. G.I. Gomero, M.J. Rebouças, and A.F.F. Teixeira, *Class. Quantum Grav.* **18**, 1885 (2001).
36. A. Bernui, and A.F.F. Teixeira, gr-qc/9904180.
37. M.J. Rebouças, *Int. J. Mod. Phys. D* **9**, 561 (2000).
38. J.-P. Uzan, R. Lehoucq, and J.-P. Luminet, *Astron. Astrophys.* **351**, 766 (1999).
39. R. Lehoucq, J.-P. Uzan, and J.-P. Luminet, *Astron. Astrophys.* **363**, 1 (2000).
40. A. Bernui, G.I. Gomero, B. Mota, and M.J. Rebouças, astro-ph/0403586.
41. A. Marecki, B.F. Roukema, S. Bajtlik, astro-ph/0412181.
42. A. Bernui and T. Villela, to appear in *Astron. Astrophys.* (2005).
43. B.F. Roukema and A. Edge, *Mon. Not. R. Astron. Soc.* **292**, 105 (1997).
44. H.V. Fagundes and E. Gausmann, *Phys. Lett. A* **261**, 235 (1999).
45. M. Lachièze-Rey and J.-P. Luminet, *Phys. Rep.* **254**, 135 (1995);  
J.J. Levin, *Phys. Rep.* **365**, 251 (2002) ;  
M.J. Rebouças and G.I. Gomero, *Braz. J. Phys.* **34**, 1358 (2004), astro-ph/0402324.
46. A. Hajian and T. Souradeep, astro-ph/05010001.
47. T. Souradeep and A. Hajian, astro-ph/0502248.
48. N.J. Cornish, D. Spergel, and G. Starkman, *Class. Quantum Grav.* **15**, 2657 (1998).

49. J. Levin, E. Scannapieco, and J. Silk, *Class. Quant. Grav.* **15**, 2689 (1998).
50. J.R. Bond, D. Pogosyan, and T. Souradeep, *Phys. Rev. D* **62**, 043005 (2000);  
J.R. Bond, D. Pogosyan, and T. Souradeep, *Phys. Rev. D* **62**, 043006 (2000).
51. A. Hajian and T. Souradeep, astro-ph/0301590.
52. A. de Oliveira-Costa, G.F. Smoot, and A.A. Starobinsky, *Astrophys. J.* **468**, 457 (1996).
53. A. de Oliveira-Costa, M. Tegmark, M. Zaldarriaga, and A. Hamilton, *Phys. Rev. D* **69**, 063516 (2004).
54. P. Dineen, G. Rocha, P. Coles, astro-ph/0404356.
55. E.P. Donoghue and J.F. Donoghue, astro-ph/0411237.
56. C.J. Copi, D. Huterer, and G.D. Starkman, astro-ph/0310511.
57. M.O. Calvão, G.I. Gomero, B. Mota, and M.J. Rebouças, astro-ph/0404536.
58. N.J. Cornish, D.N. Spergel, G.D. Starkman, and E. Komatsu, *Phys. Rev. Lett.* **92**, 201302 (2004).
59. J.-P. Luminet, J. Weeks, A. Riazuelo, R. Lehoucq and J.-P. Uzan, *Nature* **425**, 593 (2003).
60. B.F. Roukema et al., *Astron. Astrophys.* **423**, 821 (2004).
61. R. Aurich, S. Lustig, and F. Steiner, astro-ph/0412569.
62. J. Gundermann, astro-ph/0503014.
63. J.-P. Luminet, astro-ph/0501189. To appear in *Braz. J. Phys.* (2005).
64. G.I. Gomero, astro-ph/0310749.
65. A. Riazuelo, J. Weeks, J.-P. Uzan, and J.-P. Luminet, *Phys. Rev. D* **69**, 103518 (2004).